Mon. Not. R. Astron. Soc. **326,** 1315–1327 (2001)

The SuperCOSMOS Sky Survey – III. Astrometry

N. C. Hambly,[1★] A. C. Davenhall,[2] M. J. Irwin[3] and H. T. MacGillivray[1]

[1]*Wide Field Astronomy Unit, Institute for Astronomy, University of Edinburgh, Blackford Hill, Edinburgh EH9 3HJ*
[2]*Institute for Astronomy, University of Edinburgh, Blackford Hill, Edinburgh EH9 3HJ*
[3]*Cambridge Astronomy Survey Unit, Institute of Astronomy, Madingley Road, Cambridge CB3 0HA*

Accepted 2001 May 14. Received 2001 May 4; in original form 2001 March 13

ABSTRACT

In this, the third in a series of three papers concerning the SuperCOSMOS Sky Survey, we describe the astrometric properties of the data base. We describe the algorithms employed in the derivation of the astrometric parameters of the data, and demonstrate their accuracies by comparison with external data sets using the first release of data, the South Galactic Cap survey. We show that the celestial coordinates, which are tied to the International Celestial Reference Frame via the Tycho–2 reference catalogue, are accurate to better than ± 0.2 arcsec at $J, R \sim 19, 18$, rising to ± 0.3 arcsec at $J, R \sim 22, 21$, with positional-dependent systematic effects from bright to faint magnitudes at the $\sim$0.1-arcsec level. The proper motion measurements are shown to be accurate to typically $\pm 10\,\mathrm{mas\,yr^{-1}}$ at $J, R \sim 19, 18$, rising to $\pm 50\,\mathrm{mas\,yr^{-1}}$ at $J, R \sim 22, 21$, and are tied to zero using the extragalactic reference frame. We show that the zero-point errors in the proper motions are $\leq 1\,\mathrm{mas\,yr^{-1}}$ for $R > 17$, and are no larger than $\sim 10\,\mathrm{mas\,yr^{-1}}$ for $R < 17\,\mathrm{mas\,yr^{-1}}$.

Key words: astronomical data bases: miscellaneous – catalogues – surveys – astrometry – reference systems – stars: kinematics.

1 INTRODUCTION

In Paper I of this series (Hambly et al. 2001a) we describe the SuperCOSMOS Sky Survey (hereafter SSS).[1] This ambitious project ultimately aims to digitize the entire sky atlas Schmidt plate collections in three colours (*B*, *R* and *I*), one colour (*R*) at two epochs. Paper II in this series (Hambly, Irwin & MacGillivray 2001b) describes the image detection, parametrization, classification and photometric calibration techniques for the survey. In this, the third paper of the series, we describe in detail the calibration of the astrometric parameters contained within the survey data. Paper I is intended as a user guide to the SSS, while Papers II and III provide more technical details concerning the derivation and calibration of the object parameters. The first release of data consisted of $\sim$5000 square degrees of the southern sky at high Galactic latitude ($|b| > 60°$), and is known as the South Galactic Cap (SGC) survey. Although these three papers make explicit reference to SGC data, all details are generally applicable to SSS data at Galactic latitudes $|b| \geq 30°$. At low Galactic latitudes, particularly towards the Galactic Centre, crowding degrades astrometric and photometric performance.

The photographic plate material used for the SSS consist of sky-limited Schmidt photographic glass plate and film originals, or glass copies of glass originals, taken with the UK, ESO and Palomar Oschin Schmidt Telescopes – for more details, see Paper I and Morgan et al. (1992, and references therein). Leaving aside such details as object detection and parametrization (see Paper II) the solution to the problem of assigning celestial coordinates to each object requires comparison with a reference catalogue and the application of a plate model. Schmidt plate astrometry has a long history (see Section 2.1 for some references) involving reference catalogues of increasing density and precision, along with increasingly sophisticated plate models – for a concise review, see Morrison, Smart & Taff (1998). These authors question the need for a conventional plate model at all, and advocate a novel technique making use of an 'infinitely overlapping circles filter'. However, we note that they concede that, for large-scale survey work at least, a global linear plate model plus non-linear correction via an empirical plate 'mask' is appropriate. It is just such a method that we describe in Section 2.1. In Section 3 we proceed to test the astrometric solutions against CCD drift scan data encompassing plate boundaries – i.e., a test of the true external errors, both random and systematic, as a function of magnitude and plate position. Section 3 also discusses our results in comparison to extragalactic objects defining the International Celestial Reference Frame (Ma et al. 1998).

In addition to providing celestial coordinates, the SSS catalogues include proper motions. In the southern hemisphere, all objects paired between the SERC–J/EJ (first epoch, hereafter B_J) and SERC–ER/AAO–R (second epoch, hereafter R) plates have a proper motion measurement (see Section 2.2.1). The

★E-mail: N.Hambly@roe.ac.uk

[1] Data base available online at http://www-wfau.roe.ac.uk/sss

methodology for determining the proper motions closely follows that described in Evans & Irwin (1995, hereafter EI95), and is detailed in Section 2.2. Small changes made necessary by the plate material used are also described. Section 3 contains a comparison between our derived proper motion measurements against an external data set, and we analyse in some detail the relative contribution of random and systematic errors on these proper motions as a function of magnitude.

As we will describe in Section 2.1, the celestial coordinates are tied to the *Hipparcos* reference frame via the Tycho–2 catalogue. As stated in the introduction to the *Hipparcos* and Tycho Catalogues (ESA 1997) this frame is practically identical to the International Celestial Reference Frame (ICRF), and we demonstrate the level of any residual zero-point errors with respect to the ICRF in Section 3. Furthermore, our proper motion zero-point is taken from extragalactic objects, and is therefore also tied to an inertial reference frame. The advantages of such a proper motion reference frame are discussed extensively with reference to the Lick Observatory Northern Proper Motion programme (NPM) (Klemola, Jones & Hanson 1987) and are clearly demonstrated by recent results from the corresponding southern hemisphere survey, the Yale Observatory/San Juan Southern Proper Motion programme (SPM) (Platais et al. 1998; Méndez et al. 1999).

2 METHODOLOGY

All photographic material for the SSS is measured on SuperCOSMOS, a fast high-precision microdensitometer. Aspects of the system enabling highly accurate positional measurements are described in Hambly et al. (1998) and will not be repeated here, except to state that it was demonstrated that the machine has the capability to centroid isolated, well-exposed stellar images on modern fine-grained emulsions at a precision of $\sim$0.5 μm (or 33 mas at the plate scale of the Schmidt sky survey plates).

2.1 Global astrometric plate solutions

Converting the positions of stars and other objects measured on a photographic plate into celestial coordinates is a classical problem in photographic astronomy, and various techniques are available to solve it. All the techniques are based on having a grid of reference stars, with known celestial coordinates, distributed over the plate. A transformation is then defined between the measured *xy* positions and the celestial coordinates of the reference stars. It is the details of calculating the transformation which may vary between different techniques.

The SuperCOSMOS global astrometric software (hereafter XYTORADEC) uses an algorithm based on the Starlink program ASTROM (Wallace 1998). The code implementing the algorithm is partly borrowed from ASTROM and partly consists of calls to routines in SLALIB (Wallace 1999), the Starlink Positional Astronomy Library. ASTROM (and hence XYTORADEC) use a modified version of the standard, traditional technique for converting plate positions to coordinates. In this technique the catalogue coordinates of the reference stars are converted to tangent plane coordinates, adjusted for geometrical distortion (caused by the telescope optics and mechanical deformation of the plates during exposure), and a linear six-coefficient least-squares fit is made between the adjusted standard coordinates and the measured positions. Several authors have described this technique (e.g. König 1962; Taff 1981; Green 1985). In this method a simple, single, global fit is made for all the reference stars imaged on the plate. The technique used by ASTROM and XYTORADEC differs from the traditional method in that the plate centre is allowed to vary (i.e., included in the fit). An outline of the method is as follows.

First, the point on the celestial sphere at which the telescope was pointing when the plate was exposed is established. Reference star coordinates are converted to apparent (i.e., observed) coordinates in the desired system. Standard (tangent plane) coordinates, $\xi\eta$, are computed for the reference stars about the tangent point. The standard coordinates are then adjusted for the geometrical distortion where each image centroid is adjusted radially. The adjustment consists of separately multiplying each ξ and η by the factor $r/\tan r$, where $r = (\xi^2 + \eta^2)^{1/2}$ (see Murray 1983, page 196).

After applying the geometric distortion, a small systematic distortion remains between the adjusted standard coordinates and positions measured on Schmidt plates. These residuals are the well-known 'swirling patterns' seen in the residuals of linear fits made to Schmidt data (e.g. Taff et al. 1992). A set of corrections at a grid of points over the plate are prepared beforehand. A grid size of 1 cm on the plate ($\sim$10 arcmin) was chosen, since this provides sufficient resolution to accurately map out the $\sim$30-arcmin-scale, non-linear distortion expected. Different grids are used for plates originating from different Schmidt telescopes and in different wavebands. These grids are prepared by averaging the residuals over numerous plates, using this fitting procedure (but of course without these corrections). Fig. 1 shows four examples of the distortion patterns from the three Schmidt telescopes providing data for sky surveys. For the UK Schmidt J survey, the data are averaged over 200 plates containing 193 866 individual standard star residuals. The ESO Schmidt data are from 142 plates/107 346 stars, while for the Palomar Schmidt first-epoch E and second epoch R surveys the data are from 51 plates/47 101 stars and nine plates/20 814 stars respectively. In all cases, the reference catalogue used was the Tycho–2 (Høg et al. 2000). The largest non-linear effects are seen for the Palomar POSS–I E plates. This has been seen previously, and is probably a result of the design of the original plate holders used for that survey (e.g. Irwin 1994). Note that the redesign of these plate holders has resulted in much smaller non-linearities for the second-epoch survey – compare Figs 1(c) and (d). For each reference star or programme object the appropriate correction is derived by interpolating the grid at the position of the star or object. Simple bilinear interpolation is used (e.g. Press et al. 1986). The corrections are then simply added to the standard coordinates.

The standard coordinates, adjusted for mechanical and optical distortion, are then fitted to the measured positions. For a complete description of XYTORADEC, see Davenhall (2000). Section 3 illustrates typical results from the above procedure.

2.1.1 *Reference catalogue*

The SGC survey data originally made publicly available on the World Wide Web made use of the ACT reference catalogue (Urban et al. 1998). Since mid-2000, the Tycho–2 catalogue has been available (Høg et al. 2000), and all SGC astrometry was re-reduced with respect to this catalogue. SSS data are now routinely reduced with respect to the Tycho–2 reference catalogue. This compilation of 2.5 million stars reaches magnitudes $V \sim 12.5$ (90 per cent complete to $V \sim 11.5$), and has positions at mean observational epoch of $\sim$J1991.5 from the Tycho catalogue, but includes proper motions via a combination of reprocessed Tycho data and first-epoch positions from the Astrographic Catalogue and 143 other

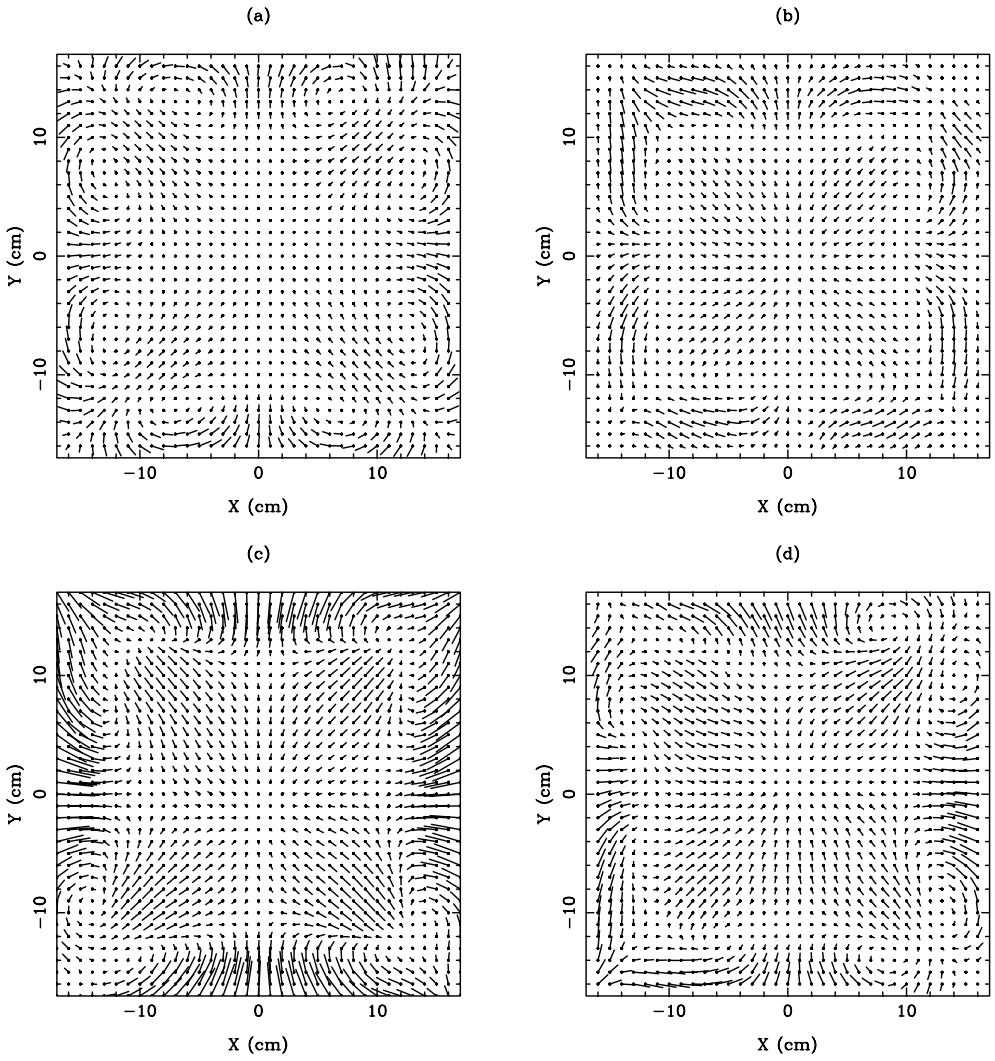

Figure 1. Mechanical deformation (or 'swirl') patterns for (a) UK Schmidt SERC−J/EJ plates, (b) ESO Schmidt R plates, (c) Palomar Schmidt first-epoch E plates and (d) Palomar Schmidt second-epoch R plates. In each case, the length of the vectors is scaled such that one tick-mark corresponds to 1 arcsec.

ground-based catalogues (see references in Høg et al.). The astrometric standard stars provided by Tycho−2 are heavily saturated on sky-limited Schmidt plates, and as we show in Section 3 that there is a demonstrable magnitude systematic between bright and faint stars at the level of up to ∼0.3 arcsec at field edges. Future projects, both ground-based (for example, the UCAC project – see Zacharias et al. 2000) and space-based, will provide higher density catalogues reaching fainter magnitudes and will bridge the magnitude range ($10.0 < V < 15.0$) required to eliminate such systematic errors from the plate solutions (e.g. Irwin et al. 1998). In this way, the full-blown *internal* precision obtainable from centroiding on Schmidt plates will ultimately limit the external accuracy of the astrometry. We note here that the SSS data base is organized in such a way as to make re-reduction of the plate astrometry easy to achieve, and when higher density catalogues become available this will indeed be done.

2.1.2 FITS world coordinate system for images extracted from the SSS data base

The availability of global astrometric plate solutions for the survey data enables any extracted FITS image (see Paper I) to contain FITS World Co-ordinate System (WCS) header information. As yet, there is no formally accepted standard method and keyword set for implementing the WCS. However, Greisen & Calabretta (1999) have proposed a standard, and we have followed this in our data base access software. The WCS is defined locally for each extracted image by fitting a linear plate model between tangent plane projected celestial coordinates and *xy* in pixel units. Large-scale, non-linear distortions are not relevant to small scales of tens of arcminutes. We simply specify the WCS using the RA−TAN and DEC−TAN prescription along with the CD rotation matrix elements (see Greisen & Calabretta 1999 for more details). This set is compatible with, for example, the Starlink software collection (e.g., image display utilities such as GAIA/SkyCAT; Draper 1999). Note also that previously defined keywords sets are also written to the FITS headers for backwards compatibility.

2.1.3 R-survey data on film

At the time of writing, it seems likely that the AAO−R survey will be completed on Kodak 4415 'Tech−Pan' film. For example, a small number (∼25) of SGC fields have film originals measured for the data base. Due to its finer emulsion granularity, this medium

is superior to IIIaF in all aspects of astronomical performance (e.g. Parker & Malin 1999; Parker et al. 2001) with the exception of large-scale astrometric stability. The 'swirl' patterns seen for glass plates (e.g. Fig. 1) do not repeat from film to film, but systematics at similar scales and of a similar amplitude are none the less present. Such fields have individual systematic correction via the corresponding J plate data. The procedure is simply to map out all plate-to-plate errors as a function of position between the R film and its corresponding SERC–J/EJ plate in a given field using the J plate to define the 'swirl' correction mask.

2.2 Proper motions

2.2.1 Choice of plate pairs and pairing criterion

The plates available for the SSS provide several potential plate pair combinations for the determination of proper motions. Any (or all) of these combinations could be used for this task. For the purposes of producing a uniform proper motion survey in the southern hemisphere to the highest possible accuracy, we chose the J/R combination for several reasons. Each field has (or soon will have) a good-quality original photograph on fine-grained emulsion reaching $J \sim 22.5$, $R \sim 21.0$. The POSS–I 'E' and ESO–R material available are glass copies, and are between 0.5 and 1.0 mag less deep; neither survey covers the entire southern hemisphere, and the POSS–I plates have the additional complication of not being on the same system of field centres as the ESO/SERC atlas. The SERC–I survey lacks depth, reaching $I \sim 19.0$. Moreover, the R survey was envisaged as a second-epoch survey to the *J*, and efforts have been made to ensure a good time baseline between the first and second epochs (Morgan et al. 1992; see, e.g., Fig. 6 later). As we show in Section 2.2.4, we can accurately model any colour effects introduced in the astrometry as a result of our choice of J/R plates. Of course, future enhancements to the SSS may include sophisticated analysis of the multiple-epoch data available from more than two plates per field if there is sufficient user demand (e.g. Paper I).

Fig. 2 shows the number of pairings made between the J and R plates for several different Galactic latitudes. These curves show the same general trends. Below a pairing criterion of 1 arcsec, a dramatic fall in the number of pairings occurs due to global positional errors (see Section 3). For a pairing criterion of more than 6 arcsec, a sudden and steady rise is seen in the number of pairings at the level of many thousands at each step. These must be spurious, since we do not expect 10^4–10^5 high proper motion stars per Schmidt field. In fact, the *total* number of stars having $\mu > 0.2$ arcsec yr^{-1} is of order 10^5 over the entire sky (Luyten 1979). A cumulative histogram of the fraction of high proper motion stars (i.e., those having $\mu > 0.2$ arcsec yr^{-1}) made from the NLTT catalogue (Fig. 3) shows that 90 per cent of those catalogued have motions $\mu < 0.4$ arcsec yr^{-1}. For a median epoch difference of 15 yr (see Fig. 6), 0.4 arcsec yr^{-1} corresponds to a shift of 6 arcsec. Hence, in order to pair 90 per cent of 'high' proper motion stars, but at the same time avoid large numbers of spurious pairings, the pairing criterion has been set at 6 arcsec. However, the data base access software (see Paper I) allows the user the default option of limiting pairings to those within 3 arcsec for most applications when completeness of high proper motion objects is not an issue. This is to further minimize the number of spurious pairings for applications that would be sensitive to such contamination – clearly, in Fig. 2 even between pairing criteria of 3 and 6 arcsec there is a rise in pairings over and above that expected from high proper motion objects alone. As far as pairing motionless objects is concerned, a pairing criterion of 3 arcsec is very generous in the light of absolute errors in position of $\sigma_{\alpha,\delta} \sim 0.3$ arcsec (Section 3).

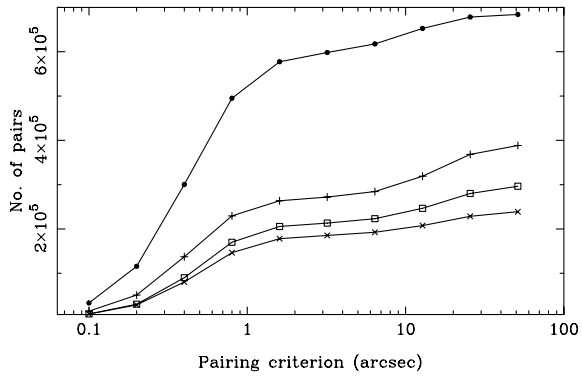

Figure 2. The number of objects paired between two plates in fields at various Galactic latitudes: $b = -32°$ (filled circles); $b = -47°$ (plus signs); $b = -65°$ (open squares) and $b = -87°$ (crosses).

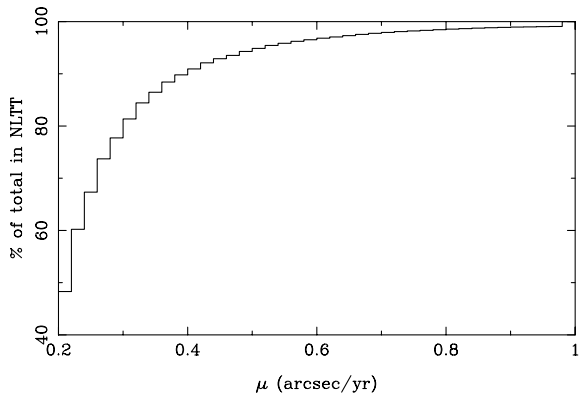

Figure 3. Cumulative histogram of the fraction of the total number of NLTT stars having a proper motion less than μ arcsec yr^{-1}. Approximately 90 per cent of NLTT stars have proper motions less than $\mu = 0.4$ arcsec yr^{-1}.

2.2.2 Plate-to-plate error mapping

The determination of accurate proper motions requires that systematic positional errors as a function of plate position be removed from the displacements of all objects measured between the first- and second-epoch plates (e.g., EI95). Such errors arise from emulsion shifts on the photographs themselves, and also from systematic positional errors during the measurement process. Note that in Hambly et al. (1998) we described a procedure for minimizing systematic measurement errors arising from the *xy* table of SuperCOSMOS; none the less, we follow EI95 exactly and compute one-dimensional error functions (i.e., errors in *x* and *y* as a function of *x* and *y*) when mapping the plate-to-plate systematic errors, since small residuals are expected to be present at the few tenths of a micron level (for example, errors resulting from pixel placement within the linear CCD used to scan the plate). Other systematic errors possibly present in the proper motions include those due to positional errors as a function of magnitude. For example, it is likely that the centroids of heavily saturated images off-axis on the photographs are displaced relative to those of fainter stars owing to off-centre haloes of scattered light, an effect compounded by the limited dynamic range of the measuring

machine. Note, however, that such effects cannot be simply measured from the data and removed, since we expect populations of objects having different mean apparent magnitudes to show systematic differences in mean proper motion due to Galactic structure (e.g., brighter stars will show systemic motions with respect to fainter stars since they are, on average, nearer to the Sun). We argue that such effects will be minimized by using the photographic material specified in the previous section, since the first- and second-epoch plates were obtained on the same field centres with the same telescope using the same guide stars at similar times of the year and at similar (optimum) airmass. Other effects due to misalignment of the scanning beam with the plate along with different 'depths' of image within the emulsion are likely to be present – e.g., EI95. In their work such effects were eliminated by measuring each plate twice, at orientations within the machine of 0° and 180°. Taking the mean position between the two scans, these errors were removed. The scale of the SSS makes scanning each plate twice impractical, and so systematic errors resulting from such effects will remain in these data.

2.2.3 *Zero-point of the proper motions*

The zero-point of the proper motion system is fixed using objects classed as galaxies (Paper II describes the image classification procedure). As described in EI95, once the plate-to-plate error mapper has removed systematic errors between the first- and second-epoch plates, in general the mean stellar displacement will be zero (since stellar images dominate the number counts), while that of galaxies will be non-zero. Simply applying a global translation to make the galaxy images have zero mean displacement fixes the proper motion zero-point to the extra-galactic frame. Note that the image classifier is reliable at the level

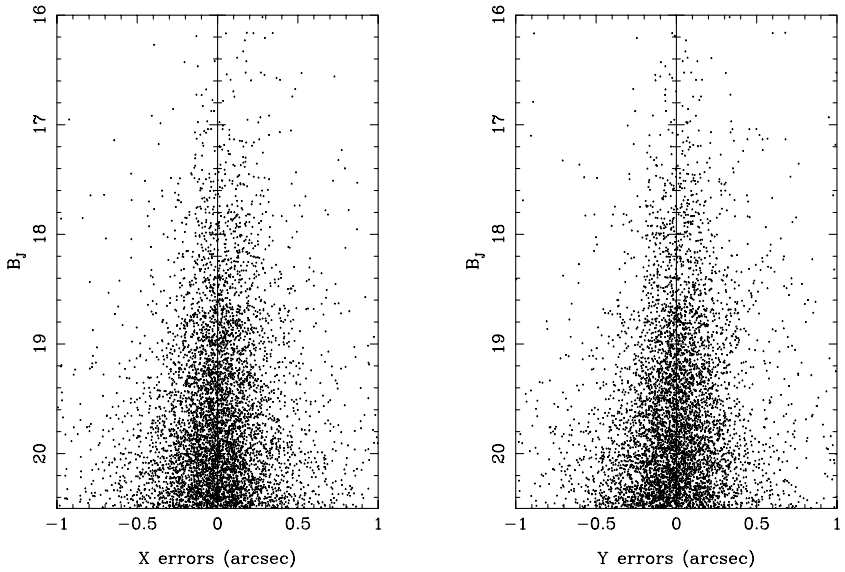

Figure 4. Distribution of residual displacement in galaxian images in *xy* as a function of magnitude for the SGP field 411, after plate-to-plate error mapping and zero-point translation between first- and second-epoch plates.

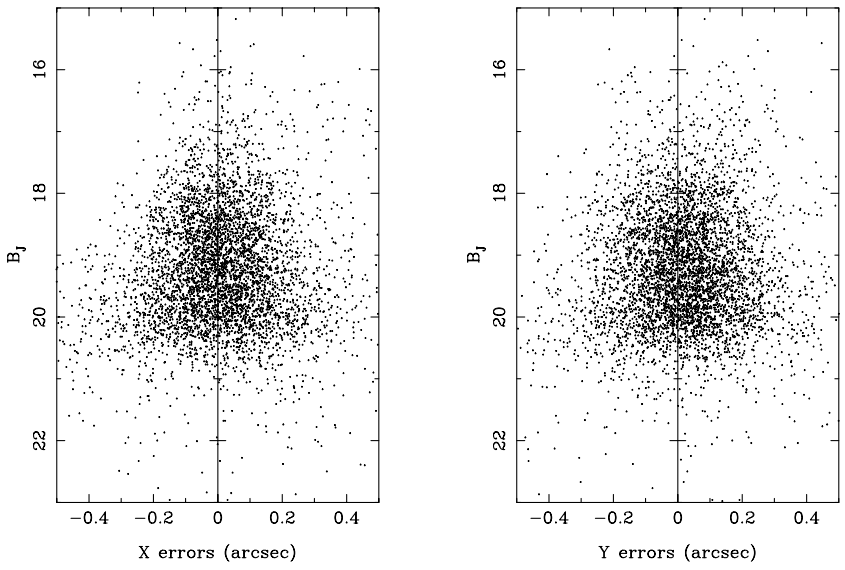

Figure 5. Distribution of residual displacement (between first- and second-epoch plates) in QSO images in *xy* as a function of magnitude for the entire SGC survey (objects catalogued in Véron-Cetty & Véron 1998). Median zero-points and rms scatter as a function of magnitude are tabulated in Table 1.

Table 1. Residual systematic zero-point errors in QSO positions between first- and second-epoch plates from Fig. 5, and implied proper motion errors (both random and systematic) for an epoch baseline of 15 yr, as a function of magnitude (however, see Section 3.2).

Magnitude range	Zero-point and rms (arcsec) RA	DEC	rms zero-point error[1] (mas yr^{-1})	$\sigma_{\mu_{\alpha,\delta}}$[1] (mas yr^{-1})
$15.5 < B_J < 16.5$	0.015 ± 0.132	0.066 ± 0.225	2.2	11.9
$16.5 < B_J < 17.5$	0.043 ± 0.137	0.052 ± 0.148	2.2	9.5
$17.5 < B_J < 18.5$	0.007 ± 0.127	0.024 ± 0.133	0.8	8.7
$18.5 < B_J < 19.5$	0.004 ± 0.132	0.019 ± 0.133	0.7	8.9
$19.5 < B_J < 20.5$	0.005 ± 0.164	0.027 ± 0.152	0.9	10.5
$20.5 < B_J < 21.5$	0.002 ± 0.242	0.016 ± 0.214	0.5	15.2
$21.5 < B_J < 22.5$	0.044 ± 0.395	-0.066 ± 0.435	2.6	27.7

[1]Assuming a median epoch difference of 15 yr.

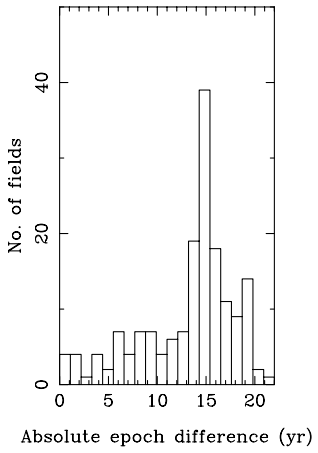

Figure 6. Histogram of epoch differences between the SGC B_J and R photographic observations.

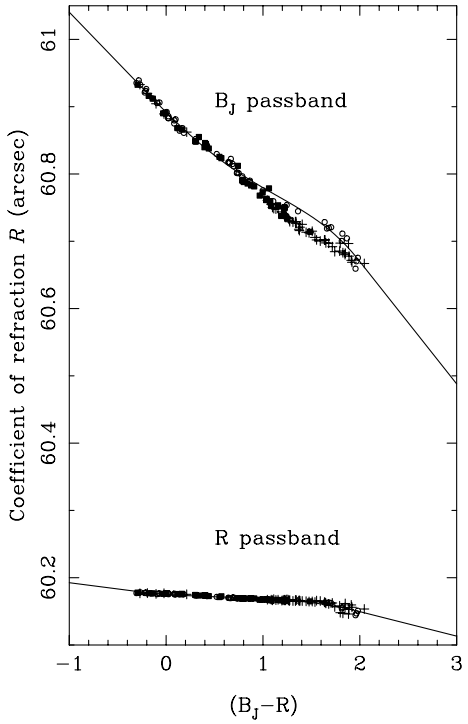

Figure 7. Computational models of R, the coefficient of refraction, as a function of $(B_J - R)$ colour. The symbol types are + for giants, filled squares for subgiants, and open circles for dwarfs. The solid lines are least-squares polynomial fits to the dwarf data, along with linear extrapolations to provide an estimate of R for any colour (cf. Evans & Irwin 1995, figs 11 and 12).

of ≥90 per cent down to $B_J \sim 20.5$ (Paper II, table 9), and so only galaxies brighter than that magnitude are used in this procedure. Fig. 4 shows an example of the distribution in galaxy displacement as a function of magnitude for the SGP field 411, demonstrating the effectiveness of this procedure. As an independent and external check on the extragalactic zero-point, we also examined the displacements of all isolated, good-quality images paired between the SGC survey data base and the Véron-Cetty & Véron (1998) QSO catalogue. Fig. 5 shows this comparison (> 5000 QSOs over the entire SGC region). Table 1 details the mean displacements and rms errors for the QSO sample. Clearly, there are no significant non-zero residuals. Moreover, this test illustrates the likely level of errors in the stellar proper motions. Fig. 6 shows a histogram of the epoch differences between the J and R survey photographs within the SGC survey. For a median epoch difference of 15 yr, the final column in Table 1 gives the implied mean proper motion precision and rms zero-point error, in either coordinate, as a function of magnitude. Obviously, some fields have much shorter time baselines than the median value, and the proper motions in such fields will be correspondingly less accurate (see Section 2.2.5).

2.2.4 Correction of systematic effects due to differential colour refraction (DCR)

As noted in EI95, differential colour refraction (DCR) corrections will be required in order that objects of different colour to the average have no systematic error in proper motions measured from plates of different bandpass. Again, these errors must not be measured from the data, since populations of different mean colour (e.g., redder young disc stars having relatively high metallicity and bluer old halo stars having relatively low metallicity) are *expected* to have different systemic motions due to their different ensemble kinematics. We modelled DCR effects following exactly the prescription given in EI95 with the necessary changes made for the different emulsion/filter combinations used here, with relevant data being taken from Evans (1989) and references therein. In Fig. 7 we show our computations of the coefficient of refraction R as a function of synthetic $(B_J - R)$ colour for the B_J and R passbands along with the polynomial fits and linear extrapolations used.

The DCR corrections are applied as detailed in equations (1) and

(2), section 5 of EI95. The corrections take the form of small changes to the second-epoch positions as a function of colour and as a function of mean galaxy colour (since the galaxies define the zero-point described above). Note that in computing the refraction coefficient we assumed nominal atmospheric temperature, pressure, humidity and unit airmass. Calculation shows that this is good enough for our purposes – for example, recomputing R for airmass χ in the range $1.0 \leq \chi \leq 2.0$ in steps of 0.1 shows negligible zero-point changes in R as a function of colour, while the gradient remains constant.

2.2.5 Proper motion error estimates

In order that some estimate of probable errors in proper motion are available when using SSS data, error values in units of mas yr^{-1} are provided with each proper motion. These errors are estimated on a field-by-field basis, and therefore take into account the small differences in survey plate quality as well as the varying time baselines. The estimates also take into account the effects of centroiding precision as a function of magnitude, individually for stars and galaxies. The measurements are made from the global average dispersions in centroids, as a function of magnitude, once the error mapping described in Section 2.2.2 has been completed. Of course, the assumption in making these estimates is that the intrinsic proper motion is small compared to the errors and makes negligible contribution to the overall dispersion. This is obviously true for galaxies and faint stars, but is an increasingly poor assumption for increasingly brighter stars. The errors are thus overestimated for bright stars.

3 RESULTS AND DISCUSSION

3.1 Positions

3.1.1 Residuals of the fitting standards

Fig. 8 shows histograms of the mean rms error per star per SGC plate in Right Ascension and Declination for the different survey plate collections included in the SSS. These plots demonstrate the ability of the plate solutions to predict the positions of the reference catalogue stars *on the plates*. It is encouraging that even for the 51 POSS–I E glass copies – which are not of the highest quality compared to modern atlas copies, and which have a mean epoch of 1954 (Minkowski & Abell 1963) – the global plate solutions are accurate at the 0.3-arcsec level.

The modal values from these histograms are in the range ~0.1 to ~0.15 arcsec, depending on survey type and excluding the POSS–I E data. The SERC–I survey gives the best results, with some mean residuals down at ~60 mas. This result is probably due to a combination of minimal proper motion errors (the mean observational epoch of the SERC–I survey is close to that of *Hipparcos*/Tycho) and also the fact that the I plates are the least sensitive of the surveys, resulting in less saturation and lower intensity scattered light haloes for the reference catalogue standards.

3.1.2 Empirical uncertainty in positions relative to the International Celestial Reference Frame (ICRF)

In a recent paper, Deutsch (1999) compared positions of a sample of extragalactic radio sources with those derived from several currently available wide-field digitized photographic survey data bases. The comparison sample came from the very long-baseline interferometric study of Ma et al. (1998), including 212 sources *defining* the ICRF. As in Deutsch (1999), we included all defining, candidate and 'other' sources from Ma et al., since their positional uncertainties are orders of magnitude smaller than those expected from photographic data. Within the SSS object catalogue data base, we matched up sources within 3 arcsec of the quoted ICRF position, but excluded poor-quality images (e.g., those near very bright stars, step-wedges or plate labels), images below Galactic latitude $|b| = 30°$ (since we are concerned with deep, sky-limited

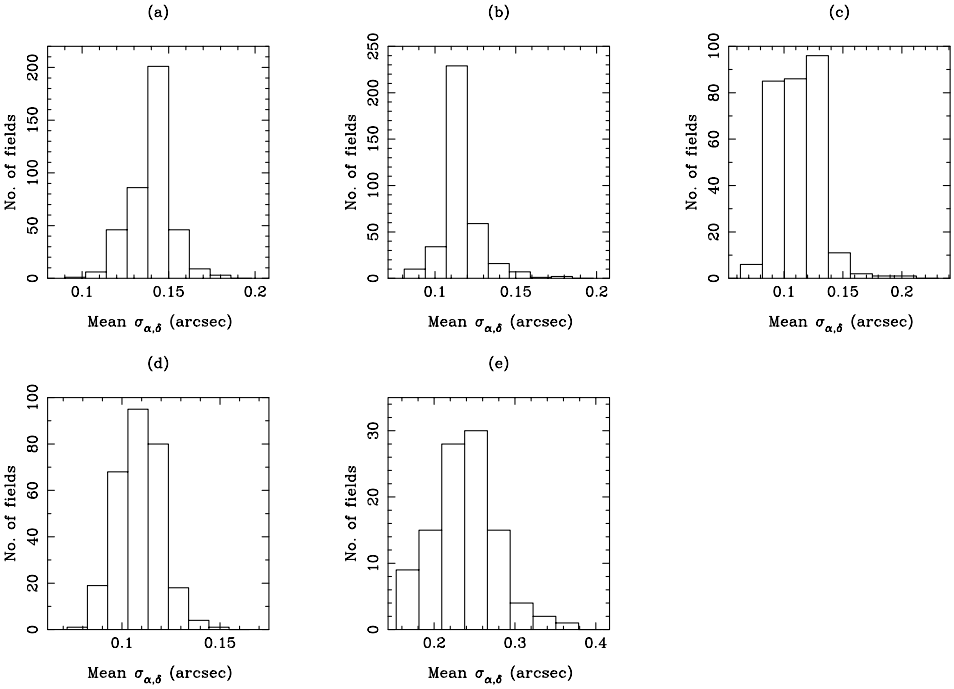

Figure 8. Histograms of the mean rms residual per star per SGC plate in either coordinate for reference catalogue (i.e., Tycho–2) stars (a) SERC J/EJ, (b) SERC ER/AAO–R (excluding data from 4415 film), (c) SERC–I, (d) ESO–R and (e) POSS–IE.

Table 2. Empirical uncertainty estimates in $|b| > 30°$ celestial positions relative to the ICRF (after Deutsch 1999). For these purposes, 'stars' refers to point-like extragalactic objects, presumably QSOs.

Survey	Object type	$\langle\Delta\alpha\rangle$ (arcsec)	$\langle\Delta\delta\rangle$ (arcsec)	N	$\Delta\alpha$ 68 per cent (arcsec)	$\Delta\delta$ 68 per cent (arcsec)	ΔR 68 per cent (arcsec)	$\Delta\alpha$ 95 per cent (arcsec)	$\Delta\delta$ 95 per cent (arcsec)	ΔR 95 per cent (arcsec)	$\Delta\alpha$ 99 per cent (arcsec)	$\Delta\delta$ 99 per cent (arcsec)	ΔR 99 per cent (arcsec)
SERC–J/	All stars	−0.054	−0.041	110	0.120	0.117	0.167	0.319	0.307	0.443	0.637	0.649	0.909
EJ	All galaxies	−0.100	0.328	5	0.145	0.456	0.478	0.502	0.880	1.013	0.502	0.880	1.013
	Stars, $B_J < 20.0$	−0.022	−0.019	92	0.108	0.108	0.152	0.238	0.241	0.338	0.313	0.317	0.445
SERC–ER/	All stars	−0.093	0.069	103	0.144	0.229	0.270	0.424	0.512	0.665	0.641	0.686	0.939
AAO–R	All galaxies	−0.117	0.187	4	0.507	0.364	0.625	0.628	0.932	1.124	0.628	0.932	1.124
	Stars, R < 18.5	−0.072	0.079	82	0.152	0.224	0.271	0.278	0.405	0.491	0.402	0.502	0.644
SERC–I	All stars	−0.160	0.081	54	0.224	0.312	0.384	0.565	0.554	0.791	1.098	1.339	1.732
	All galaxies	−0.135	−0.304	7	0.170	0.251	0.303	0.462	0.631	0.782	0.462	0.631	0.782
	Stars, I < 17.0	−0.110	0.113	21	0.121	0.284	0.309	0.324	0.474	0.575	0.347	0.548	0.648
ESO–R	All stars	0.083	0.135	38	0.133	0.173	0.218	0.283	0.316	0.424	0.450	0.398	0.600
	All galaxies	0.365	0.381	2	0.251	0.235	0.344	0.251	0.267	0.367	0.251	0.267	0.367
	Stars, R < 18.0	0.096	0.146	23	0.134	0.178	0.223	0.355	0.305	0.468	0.437	0.386	0.583
POSS–I E	All stars	0.130	−0.059	22	0.328	0.312	0.453	1.235	1.336	1.819	1.563	1.752	2.348
	Stars, E < 17.5	0.172	−0.005	6	0.141	0.194	0.240	0.333	0.510	0.609	0.333	0.510	0.609

plates) and deblended images (whose centroids will be, in general, systematically wrong – e.g. Beard, MacGillivray & Thanisch 1990). Table 2 shows the results of the comparison, where we have split the sample into stars (for 'stars' in this discussion we are referring to extragalactic objects classed as stellar in SSS catalogues – presumably these are QSOs) and galaxies, since image centroiding is in general a factor of ∼2 less accurate for galaxies than for stars (e.g. Irwin 1985). We also provide figures for stellar samples more than 2.5 mag above the respective plate limits where the random errors due to emulsion noise are reasonably small and constant (e.g. Lee & van Altena 1983). We give results equivalent to those in Deutsch (1999), for each of the survey types, to enable direct comparison: columns 3 and 4 of Table 2 show the median zero-point of the respective samples (described by columns 1 and 2) with respect to the ICRF; column 5 gives the number of objects in each sample; columns 6 to 14 are grouped in triplets, each set of three showing the maximum deviation in α, δ and $R[= (\alpha^2 + \delta^2)^{1/2}]$ for the best 68, 95 and 99 per cent of the samples.

Comparing the numbers in Table 2 with corresponding values in table 1 of Deutsch (1999), the accuracy of the SGC survey global astrometry is clearly as good as any other data base for the same survey material. Table 2 also clearly demonstrates that, globally at least, the astrometry of point-like sources has no zero-point errors with respect to the ICRF larger than ∼100 mas for many of the plate collections. In the worst cases (e.g., POSS–I E, ESO–R) the global zero-point errors are no larger than ∼200 mas. Note that these comparison objects have magnitudes in the range $15 < R < 19$ (e.g. Deutsch 1999, fig. 1d) while the reference catalogue stars have $R < 12$. Note also that some proportion of the apparently random errors listed in Table 2 will manifest themselves as local, systematic position errors (see the next section).

3.1.3 Local position errors as a function of magnitude and plate position

As stated earlier, it is important to investigate systematic errors as a function of magnitude and plate position, since the external reference catalogue standards are highly saturated on the survey photographs. Off-centre scattered light haloes inevitably 'pull' the centroids of these stars (as measured by the scanning machine) in a radial direction from the plate centre. The direction of this shift on the celestial sphere will be discontinuous as one moves from using positional data in one field to that in an adjacent field; the amplitude of this discontinuity will also vary with magnitude. The discontinuities in systematic errors with respect to external data are likely to be highest in fainter magnitude ranges for global astrometric fits based on bright standards.

Stone, Pier & Monet (1999) provide the means to measure the size of such systematic effects via comparison with their CCD drift-scan data in the Sloan Digital Sky Survey calibration regions. These regions consist of equatorial strips of ∼7.°5 in Right Ascension and ∼3.°5 in Declination, with typical astrometric accuracy quoted as ∼35 mas at $R = 10.0$ degrading to ∼70 mas at $R = 18.0$. Figs 9 and 10 show the results of this comparison for the R data in the ranges $10 < R < 14$ and $14 < R < 18$ respectively, for calibration region 'A' which falls over survey fields 824 to 826. The extent of the individual field data are indicated in the plots, where a 'seamless' catalogue has been extracted from the data base as detailed in Paper I. Data from the >10 000 objects in common have been binned into boxes ∼20 arcmin on a side and smoothed/filtered on a 3 × 3 bin scale for the purposes of display in Figs 9(e) and 10(e).

Once again, we find no large systematic offset between the SGC coordinates and those of Stone et al. (1999). The random errors are also consistent with those from Table 2, and are estimated from the distributions in Figs 9 and 10, (a) and (c) to be in the range $0.10 < \sigma_{\alpha,\delta} < 0.16$ arcsec. Figs 9 and 10 (e) demonstrate the level of systematic differences as a function of magnitude (error vectors are scaled such that $1° \equiv 1$ arcsec). A discontinuity in the vector direction can clearly be seen in Fig. 10(e) when moving from field 826 to 825; the level of this discontinuity is several tenths of an arcsecond. In any application having a tight error budget (e.g., fibre spectroscopy with very small diameter fibres, say 0.5 arcsec or smaller) one should be careful when using these data across a field boundary. We note, however, that for 2dF applications (i.e., 2-arcsec diameter fibres over 2.°0; Gray et al. 1993) these data have the requisite astrometric precision.

The residuals seen in Fig. 9(e) at $X \sim 3.°0$, $Y \sim -1.°5$ illustrate how potentially misleading the histograms in Fig. 8 can be for

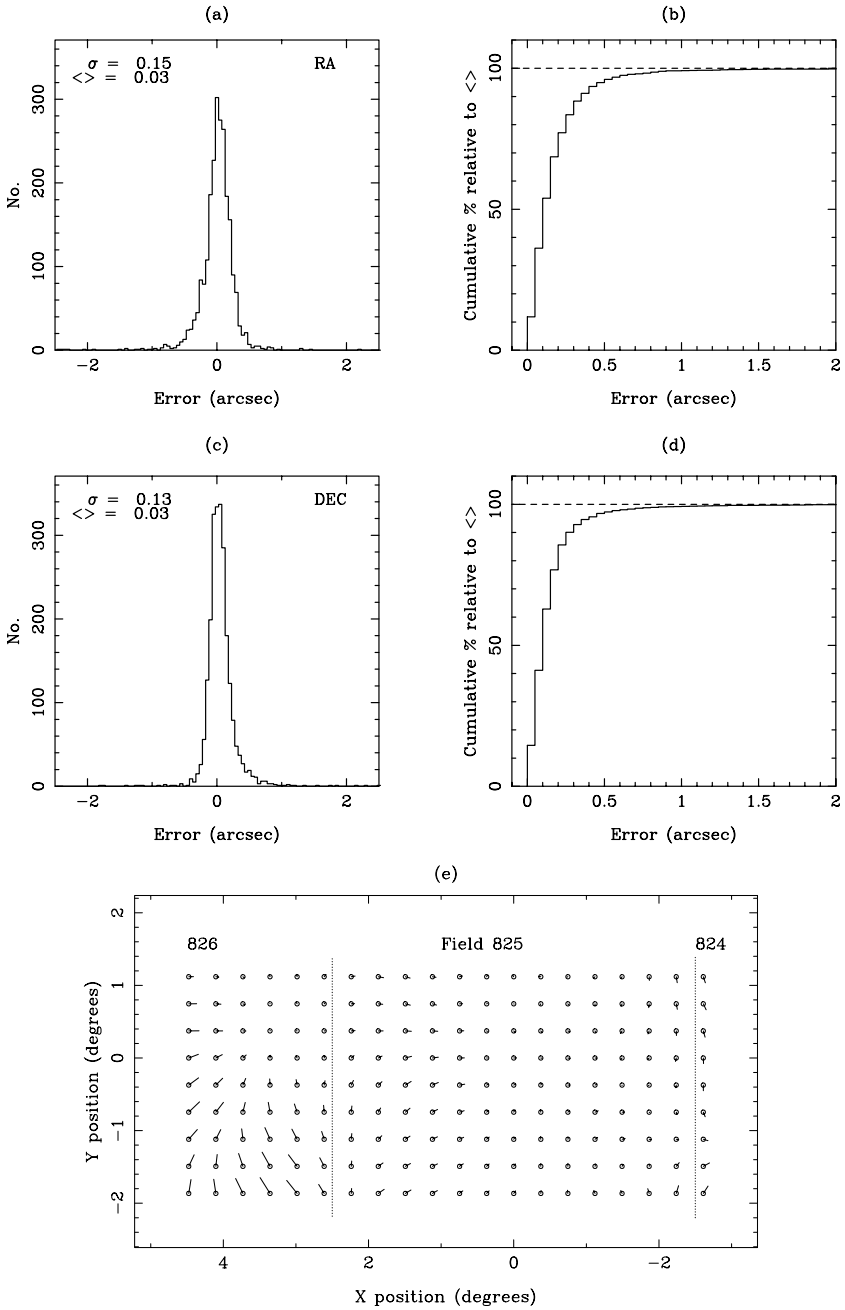

Figure 9. Comparison against SDSS CCD calibration region 'A' data (field centre RA $\sim 0^{\rm h}40^{\rm m}$, Dec. $\sim 0°$) from Stone et al. (1999) in the magnitude range $10 < R < 14$. In (e), the systematic error vectors have been scaled such that 1 arcsec $\equiv 1°$. Dotted lines indicate the field data boundaries.

estimating true external errors in the celestial coordinates. Clearly, there are systematic discrepancies in SGC survey astrometry on scales of 1 deg or so and at the level of up to ~0.3 arcsec that are not apparent from the residuals of the individual field astrometric fits. We reiterate that Fig. 8 merely shows how well the astrometric fits model how the reference stars appear on the plate to the measuring machine, and *not necessarily* where they are on the celestial sphere.

The standard errors of $\sigma_{\alpha,\delta} \sim 0.1$ arcsec in Figs 9 and 10, (a) and (c) are dominated by those for the most numerous, faint stars at $R \sim 18.5$. Towards the plate limits, object centroiding becomes less accurate due to emulsion noise (e.g. Lee & van Altena 1983), and we expect that the errors in positions will increase with magnitude (e.g. Hambly et al. 1998, fig. 8) such that at the plate limits of $R \sim 21$ the random errors will be $\sigma_{\alpha,\delta} \sim 0.3$ arcsec.

3.2 Proper motions

Platais et al. (1998) describe the Yale/San Juan SPM programme, from which the first release of data contains proper motions of 58 880 objects (defined by a set of input catalogues) around the South Galactic Pole (SGP). The typical accuracies of their data range from ~3 mas yr^{-1} at $V < 15$ to ~8 mas yr^{-1} at $V = 18.5$.

Figs 11 and 12 show straight forward comparisons between SPM and SGC proper motions in four magnitude ranges: $10 < V \leq 14$, $14 < V \leq 16$, $16 < V \leq 17.5$ and $17.5 < V \leq 18.5$ (the last is

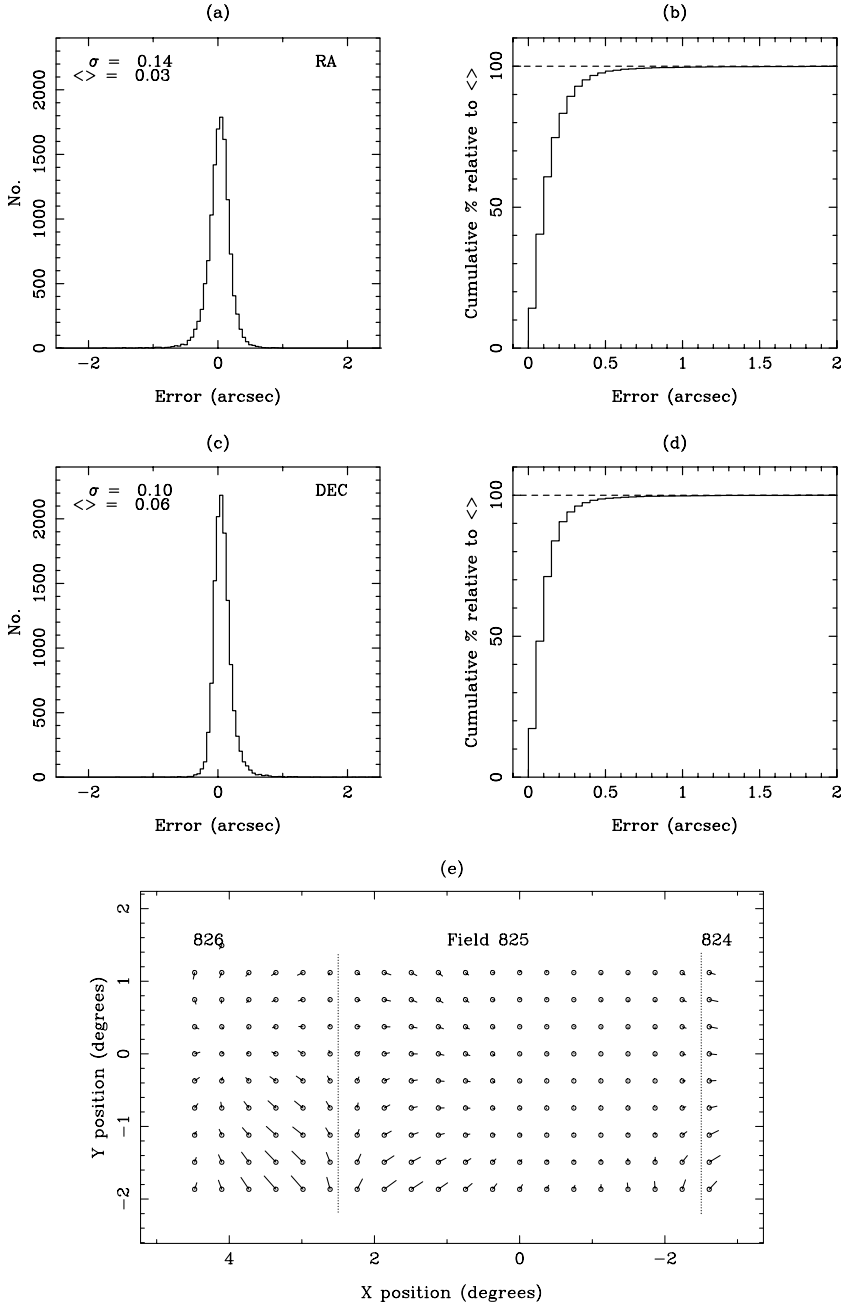

Figure 10. Comparison against SDSS CCD calibration region 'A' data (field centre RA $\sim 0^{h}40^{m}$, Dec. $\sim 0°$) from Stone et al. (1999) in the magnitude range $14 < R < 18$. In (e), the systematic error vectors have been scaled such that 1 arcsec $\equiv 1°$. Dotted lines indicate the field data boundaries.

Table 3. Quantitative comparison between SGC and SPM proper motions (see text).

Magnitude range	$\mu_\alpha \cos(\delta)$ zp and σ (mas yr^{-1})		μ_δ zp and σ (mas yr^{-1})		$\sigma_{\mu_\alpha \cos(\delta)}$[1] (mas yr^{-1})	σ_{μ_δ}[1]
$10.0 < V < 14.0$	10.0	9.5	−12.4	8.2	16.4	18.9
$14.0 < V < 16.0$	8.5	8.5	−10.3	7.8	13.8	15.9
$16.0 < V < 17.5$	3.9	9.6	−5.4	9.1	10.7	11.3
$17.5 < V < 18.5$	0.8	14.3	−1.8	14.1	14.2	14.3

[1]'Effective' global random error including zero-point (zp) error.

limited by the SPM data). It is immediately apparent that there are magnitude-dependent systematic errors in the SGC proper motions of brighter stars. Table 3 quantifies these zero-point errors for the SGP region, and also gives the scatter between the SGC and SPM data. Given the level of random error quoted in Platais et al. (1998), these values should be dominated by errors in the SGC measurements.

Comparing with Fig. 5 and Table 1, there is a consistent

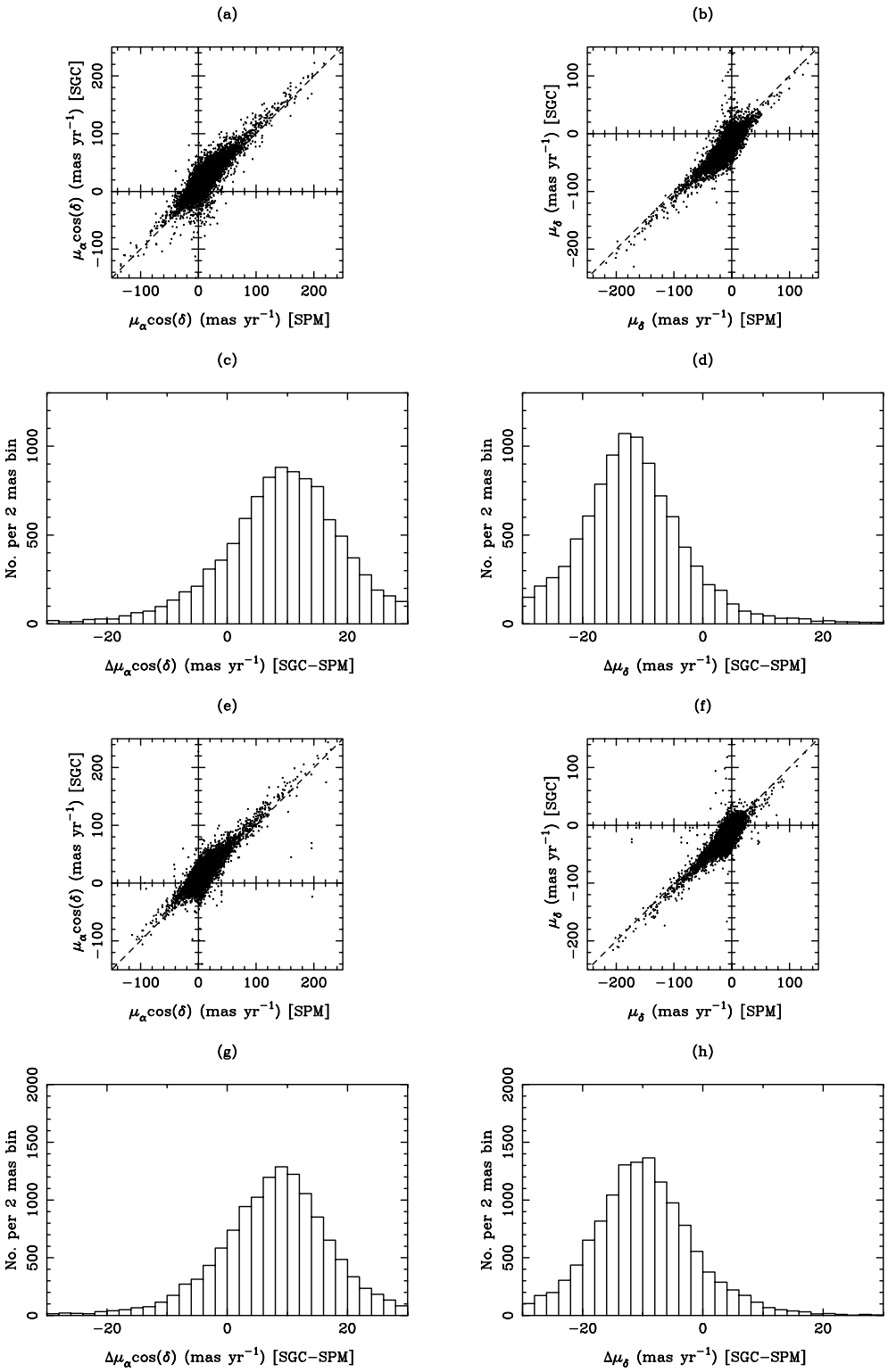

Figure 11. Comparison of SGC proper motions versus those from SPM; (a) to (d) are for $10.0 < V < 14.0$, (e) to (h) for $14.0 < V < 16.0$.

picture of no magnitude systematics for $m \geq 17.5$. However, brighter magnitude ranges in Table 1 fail to indicate true zero-point errors. This underestimate is due to the fact that the data cover the whole SGC survey region, and systematic zero-points of different magnitude and sign manifest themselves as an increased random error. On the other hand, because the SGC−SPM comparison is done in a restricted declination range near the SGP, there is a clearer tendency for systematic zero-points of the same magnitude and sign. The global random errors for SGC proper motions are therefore dominated by magnitude-dependent systematics for $V < 17$, and Table 3 indicates this by measuring the apparent SGC−SPM scatter

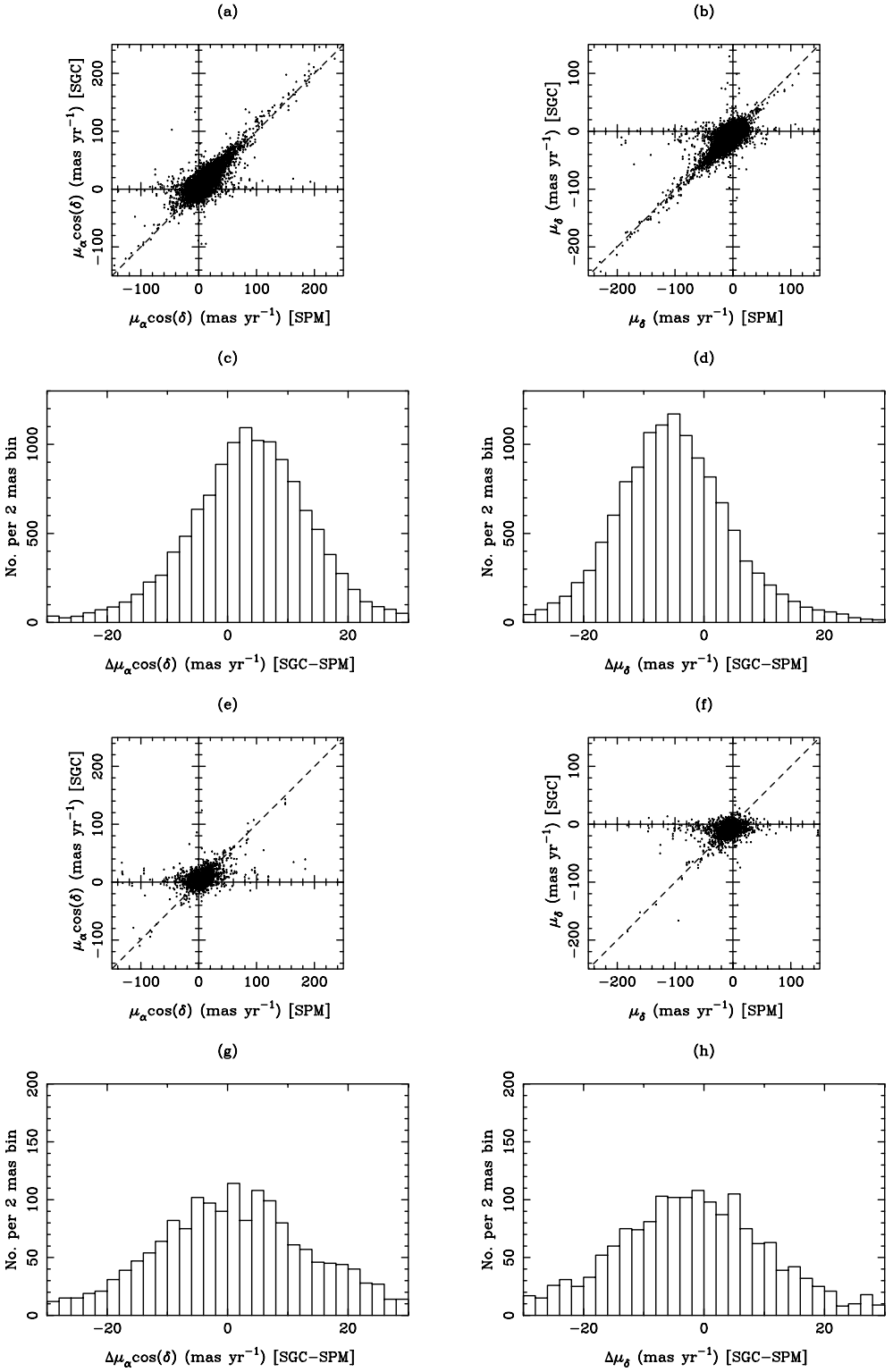

Figure 12. Comparison of SGC proper motions versus those from SPM; (a) to (d) are for $16.0 < V < 17.5$, (e) to (h) for $17.5 < V < 18.5$.

without removal of zero-point errors. Application of a global correction to the proper motions to remove these zero-point errors is clearly not possible, since their magnitude and sign changes over the SGC region. Once again, centroiding errors will increase with magnitude as one approaches the plate limits such that at $J, R \sim 22, 21$ the proper motion errors will be $\sim$50 mas yr^{-1}, but with a zero-point error with respect to the extragalactic frame of $\leq$1 mas yr^{-1}.

4 CONCLUSIONS

We have presented a detailed description of the astrometric

properties of the SuperCOSMOS Sky Survey (SSS). Using the first release South Galactic Cap (SGC) data, we have demonstrated the level of random errors in positions and proper motions by comparison SGC survey with external data; moreover, we have demonstrated the level of any systematic effects in these astrometric parameters as a function of magnitude, and in the case of positions as a function of field position. For a summary of these results, along with similar comparisons for other large-scale survey programmes and a guide to using the SSS data base, the reader is referred to Paper I.

ACKNOWLEDGMENTS

We thank Ron Stone for providing the SDSS data in advance of publication and in machine-readable form. We also thank Russell Cannon, Sue Tritton, Mike Read and Patrick Wallace for useful discussions. NCH thanks Peter Draper for advice concerning FITS WCS keywords and the use of GAIA. Funding for the University of Edinburgh Institute for Astronomy Wide-Field Astronomy Unit and Institute of Astronomy Cambridge Astronomical Survey Unit is provided by the UK PPARC. This research has made use of data archived at the CDS, Strasbourg. We acknowledge the use of Starlink computer facilities at Edinburgh and Leicester. We are indebted to the referee, Sean Urban, for a prompt and thorough review of our manuscripts.

The National Geographic Society–Palomar Observatory Sky Survey (POSS–I) was made by the California Institute of Technology with grants from the National Geographic Society. The UK Schmidt Telescope was operated by the Royal Observatory Edinburgh, with funding from the UK Science and Engineering Research Council (later the UK Particle Physics and Astronomy Research Council) until 1988 June, and thereafter by the Anglo-Australian Observatory. The blue plates of the Southern Sky Atlas and its equatorial extension (together known as the SERC–J/EJ) as well as the Equatorial Red (ER), the second-epoch (red) Survey (SES or AAO–R) and the infrared (SERC–I) Survey were taken with the UK Schmidt Telescope. All data retrieved from URLs described herein are subject to the copyright given in this copyright summary. Copyright information specific to individual plates is provided in the downloaded FITS headers.

REFERENCES

Beard S. M., MacGillivray H. T., Thanisch P. F., 1990, MNRAS, 247, 311
Davenhall A. C., 2000, 'Programmer's Note for XYTORADEC' – see ftp://ftp.roe.ac.uk/pub/scos/xytoradec.ps
Deutsch E. W., 1999, AJ, 118, 1882
Draper P. W., 1999, Starlink User Note No. 214.5, GAIA – Graphical Astronomy & Image Analysis Tool. CCLRC/Rutherford Appleton Laboratory, PPARC
ESA, 1997, The *Hipparcos* and Tycho Catalogues, ESA SP–1200. ESA, Noordwijk
Evans D. W., 1989, A&AS, 78, 249
Evans D. W., Irwin M., 1995, MNRAS, 277, 820 (EI95)
Gray P. M., Taylor K., Parry I. R., Lewis I. J., Sharples R. M., 1993, in Gray P. M., ed., ASP Conf. Ser. Vol. 37, Fibre Optics in Astronomy II. Astron. Soc. Pac., San Francisco, p. 145
Green R. M., 1985, Spherical Astronomy. Cambridge Univ. Press, Cambridge
Greisen E. W., Calabretta M., 1999, preprint (September 24) – see ftp://ftp.cv.nrao.edu/NRAO-staff/egreisen/wcs.ps.gz
Hambly N. C., Miller L., MacGillivray H. T., Herd J. T., Cormack W. A., 1998, MNRAS, 298, 897
Hambly N. C. et al., 2001a, MNRAS, 326, 1279 (Paper I, this issue)
Hambly N. C., Irwin M. J., MacGillivray H. T., 2001b, MNRAS, 326, 1295 (Paper II, this issue)
Høg E. et al., 2000, A&A, 355, L27
Irwin M. J., 1985, MNRAS, 214, 575
Irwin M. J., 1994, IAU Working Group on Wide-Field Imaging Newsletter No. 5. p. 25
Irwin M. J., Hawkins M. R. S., Hambly N. C., MacGillivray H. T., 1998, Anglo-Australian Observatory Newsletter No. 85 (April 1998). p. 14
Klemola A. R., Jones B. F., Hanson R. B., 1987, AJ, 94, 501
König A., 1962, in Hiltner W. A., ed., Astrometry with Astrographs.Chapter 20 Univ. Chicago Press, Chicago
Lee J.-F., van Altena W. F., 1983, AJ, 88, 1683
Luyten W. J., 1979, NLTT Catalogue. Univ. Minnesota Press, Minneapolis
Ma C. et al., 1998, AJ, 116, 516
Méndez R. A., Platais I., Girard T. M., Kozhurina-Platais V., van Altena W. F., 1999, ApJ, 524, L39
Minkowski R. L., Abell G. O., 1963, in Strand K. A. ed., Stars and Stellar Systems Vol. III: Basic Astronomical Data. Univ. Chicago Press, Chicago, p. 481
Morgan D. H., Tritton S. B., Savage A., Hartley M., Cannon R. D., 1992, in MacGillivray H. T., Thomson E. B. eds, Digitised Optical Sky Surveys. Kluwer, Dordrecht, p. 11
Morrison J. E., Smart R. L., Taff L. G., 1998, MNRAS, 296, 66
Murray C. A., 1983, Vectorial Astrometry. Adam Hilger, Bristol
Parker Q. A., Malin D. F., 1999, Proc. Astron. Soc. Aust., 16, 288
Parker Q. A., Malin D. F., Cannon R. D., Phillipps S., Russell K. S., 2001, MNRAS, submitted
Platais I. et al., 1998, AJ, 116, 2556
Press W. H., Flannery B. P., Teukolsky S. A., Vetterling W. T., 1986, Numerical Recipes – The Art of Scientific Computing. Cambridge Univ. Press, Cambridge
Stone R. C., Pier J. R., Monet D. G., 1999, AJ, 118, 2488
Taff L. G., 1981, Computational Spherical Astronomy. John Wiley & Sons, New York
Taff L. G., Lattanzi M. G., Bucciarelli B., Daou D., 1992, in MacGillivray H. T., Thomson E. B., eds, Digitised Optical Sky Surveys. Kluwer, Dordrecht, p. 185
Urban S. E., Corbin T. E., Wycoff G. L., 1998, AJ, 115, 2161
Véron-Cetty M. P., Véron P., 1998, ESO Scientific Report Series Vol. 18. European Southern Observatory, Garching
Wallace P. T., 1998, Starlink User Note No. 5.17: ASTROM – Basic Astrometry Program. CCLRC/Rutherford Appleton Laboratory, PPARC
Wallace P. T., 1999, Starlink User Note No. 67.45: SLALIB: Positional Astronomy Library. CCLRC/Rutherford Appleton Laboratory, PPARC
Zacharias N. et al., 2000, AJ, 120, 2131

This paper has been typeset from a TEX/LATEX file prepared by the author.